

Gas accretion from minor mergers in local spiral galaxies

E. M. Di Teodoro¹ and F. Fraternali^{1,2}

¹ Department of Physics and Astronomy, University of Bologna, 6/2, Viale Berti Pichat, 40127 Bologna, Italy

² Kapteyn Astronomical Institute, Postbus 800, 9700 AV Groningen, The Netherlands

ABSTRACT

In this paper we quantify the gas accretion rate from minor mergers onto star-forming galaxies in the Local Universe using H I observations of 148 nearby spiral galaxies (WHISP sample). We developed a dedicated code that iteratively analyses H I data-cubes, finds dwarf gas-rich satellites around larger galaxies and estimates an upper limit to the gas accretion rate. We found that 22% of the galaxies have at least one detected dwarf companion. We made the very stringent assumption that all satellites are going to merge in the shortest possible time transferring all their gas to the main galaxies. This leads to an estimate of the maximum gas accretion rate of $0.28 M_{\odot} \text{ yr}^{-1}$, about five times lower than the average SFR of the sample. Given the assumptions, our accretion rate is clearly an overestimate. Our result strongly suggests that minor mergers do not play a significant role in the total gas accretion budget in local galaxies.

Key words. galaxies: dwarfs – galaxies: evolution – galaxies: interactions – galaxies: star formation

1. Introduction

The evolution of galaxies is strongly affected by their capability of retaining their gas and accreting fresh material from the surrounding environment. Galaxies belonging to the so-called “blue-sequence”, which are actively forming stars and are dominated by young stellar populations, show an almost constant or a slowly declining star formation rate (SFR) throughout the Hubble time (e.g., Panter et al. 2007). Since the gas consumption time-scales are always of the order of a few Gyrs (Noeske et al. 2007; Bigiel et al. 2011), spiral galaxies need to replenish their gas at rates comparable to their star formation rates (Hopkins et al. 2008; Fraternali & Tomassetti 2012). These arguments are fully applicable to the Milky Way: with a SFR of 1-3 M_{\odot} slowly declining over the last ~ 10 Gyrs (e.g., Aumer & Binney 2009; Chomiuk & Povich 2011), the Galaxy would have exhausted its gas reservoir in a few Gyrs without replacement from outside (e.g., Chiappini et al. 1997).

There are essentially two sources from which disc galaxies can gain new gas: the intergalactic medium (IGM) and other gas-rich galaxies. The IGM is the place where the most of baryons are thought to still reside (e.g., Bregman 2007). Most of this gas should be in a diffuse warm-hot phase (e.g., Shull et al. 2012). Therefore the IGM represents a huge reservoir of nearly pristine gas but how this material can cool and accrete onto the discs is not well understood. Current cosmological simulations predict that gas accretion can occur in two modes (e.g., Ocvirk et al. 2008; Kereš et al. 2009): the “hot” accretion, which dominates the growth of massive galaxies, and the “cold” accretion through filamentary streams and clouds, which prevails in lower mass structures and at high redshifts (e.g., Dekel & Birnboim 2006).

The second channel for gas accretion is given by merger events. According to the Extended Press-Schechter theory, the structures in the Universe grow by several inflowing events and have increased their mass content through a small number of major mergers, more common at high redshifts, and through an almost continuous infall of dwarf galaxies (Bond et al. 1991;

Lacey & Cole 1993). Although several theoretical (e.g., Stewart et al. 2009; Kazantzidis et al. 2009) and observational studies (e.g., Patton et al. 2000; Lotz et al. 2008; Lambas et al. 2012) have been carried out in the last years, the predictions and the estimates for the galaxy merger rate and its evolution with redshift remain uncertain and no consensus has been achieved yet (e.g., Bertone & Conselice 2009; Hopkins et al. 2010).

In this paper, we use neutral hydrogen (H I) observations to investigate gas accretion from minor mergers onto star-forming galaxies in the Local Universe. The advantage of using H I observations instead of the optical-UV ones is that both morphological and kinematical information are immediately available. In addition, the gas layers are more easily disturbed by tidal interactions than the stellar disc. Two recent studies, namely Holwerda et al. (2011) and Sancisi et al. (2008), have taken advantage of H I data and both make use of the WHISP catalogue (van der Hulst et al. 2001). Holwerda et al. (2011) focused on the galaxy merger fraction and, employing techniques developed for optical-UV observations, found a merger fraction between 7% and 13%. Instead, Sancisi et al. (2008) attempted to quantify the contribution of minor mergers to the total gas accretion. They found that 25% of local galaxies show signs of minor interactions or have disturbed H I distribution and, assuming lifetimes for these observed features of about 1 Gyr and typical accreted H I mass of order 10^8 - $10^9 M_{\odot}$, they calculated an accretion rate of about 0.1 - $0.2 M_{\odot} \text{ yr}^{-1}$. This value is about an order of magnitude lower than typical star formation rates.

In this study, we use a quantitative approach to obtain a reliable estimate for the merger fraction and the gas accretion rate. We make use of a specific-purpose numerical code that is able to quickly analyse a large number of H I data-cubes, find dwarf gas-rich companions around disc galaxies and estimate an upper limit for the gas accretion onto the discs. In section 2, we describe the main features of our code and the methods adopted. In section 3, we show the results obtained by applying our analysis on a sub-sample of the WHISP catalogue and we discuss them in section 4.

2. Method

We wrote a numerical code to automatically identify 3D sources in data-cubes, i.e. image arrays with two spatial dimensions, related to the position on the plane of the sky, and one spectral dimension, which can correspond either to velocity or to frequency. Our code is targeted to work with H_I observations as it performs a three dimensional scanning of the data to look for dwarf gas-rich companions around large galaxies. Once the program has found a candidate, it derives its physical properties, such as the H_I mass, the projected distance from the main galaxy and an estimate of the accretion rate onto the central disc. In short, the code used in this work is essentially a source finder plus an algorithm for estimating the accretion rate.

The standard flow of our code can be outlined in three steps:

1. *Identifying the main-galaxy.* The pixels referable to the central galaxy emission are identified and isolated through an appropriate mask.
2. *Searching for dwarf galaxies.* The data-cube is scanned for three-dimensional sources and dwarf galaxies or H_I clouds inside the field of view are identified.
3. *Estimating the gas accretion rate.* For each detected dwarf, a maximum accretion rate onto the disc is calculated by estimating a minimum time of collision between the satellite and the central galaxy.

In the following sections, we describe the most important steps and the main features and limitations of our code.

2.1. Searching for sources and background statistics

The searching algorithm is derived from *Duchamp*, a code dedicated to three-dimensional source detection (Whiting 2012) and developed for the Australian SKA Pathfinder (ASKAP). The basic idea behind this algorithm is to locate and connect groups of bright and contiguous pixels that lie above some flux threshold, without imposing any size or shape requirement to the detection. The search is performed using either a two-dimensional raster-scanning algorithm (Lutz 1980) or a one-dimensional research along each individual pixel spectrum. Three-dimensional sources (two spatial dimensions and one spectral) are then built up on the basis of adjacency or neighbourhood criteria both in the velocity and in the spatial domain. For a full description of the source finding algorithm, we refer to the *Duchamp* main paper. The one-dimensional technique is less computationally expensive, but it can bring to spurious detections. On the contrary, the Lutz algorithm is generally more reliable at the price of the computational slowness. As discussed later in this section, we used the 1-D method to identify the main galaxy emission and the 2-D technique to detect companions.

The searching algorithm can be schematically summarized as follows:

1. *Pixel detection.* The data-cube is scanned using one of the above mentioned techniques and a list of all pixels with a flux greater than a given threshold is produced.
2. *Merging objects.* The detected pixels that are considered close to each other based on spatial and spectral requirements are merged together. Adjacent detections or detections lying within a user-defined range of pixels or channels are expected to belong to the same object. After this step, a list of three-dimensional sources is produced.

3. *Growing objects.* The size of the detections is increased by adding pixels at the edges of the objects that are above some secondary threshold. This step guarantees a smooth transition between the source and the background.
4. *Rejecting objects.* Not all detected objects can be considered reliable. Sources that do not match some agreement criteria, like a minimum number of contiguous pixels and channels, are discarded.

A crucial point of the searching algorithm is the determination of the flux threshold above which a pixel can be considered as a part of a source. In order to do this, the code needs to estimate the central value and width of the noise distribution in the data-cube. The former should be zero or very close to zero for H_I data-cubes without systematics (due for instance to problems with the data reduction). The typical data-cube of the WHISP survey is dominated by a large number of noise pixels and a relatively small number of bright pixels that belong to the sources. In such a situation, it is preferable to calculate the noise over the whole data-cube using the median as noise middle and the median absolute deviation from the median (MADFM, hereinafter) as noise spread. These quantities are less sensitive to the presence of very bright pixels than the equivalent normal statistics, the mean μ and the standard deviation σ . For a Gaussian distribution, the standard deviation can be written in term of the MADFM as $\sigma = s/0.6745$ (for details, see Whiting 2012, and references therein). The threshold τ is then determined with a simple sigma-clipping, i.e., it is set at a number n of standard deviations σ above the median m :

$$\tau = m + n\sigma \quad (1)$$

Such a value is the minimum flux that a pixel must possess to be selected by the algorithm. We checked that the noise middle and spread calculated using the whole data-cube are the same as those obtained using only the channels with line emission; the differences do not exceed 5%.

We used the searching algorithms in two different steps: the identification of the main galaxy and the detection of satellites. The former consists in isolating all those regions ascribable to the main galaxy emission. The code performs a search in the data-cube using the one-dimensional technique and selects as the main galaxy the object that covers the largest number of pixels. This approach is not computationally expensive, and it is reliable when the code is analysing an heterogeneous group of galaxies, but it does not allow the code to identify systems in advanced phase of merging, i.e., when a companion is physically connected in space and velocity with the main galaxy. Concerning the satellites, we used the Lutz algorithm, which guarantees a better reliability and minimizes the number of spurious detections. We impose a neighbourhood criterion grounded on the spatial and spectral resolution of the observations: each detected pixel is merged with other detected pixels lying within a spatial beam and within two velocity channels, which is the typical instrumental broadening (FWHM) for H_I observations when Hanning smoothing has been applied. Finally, we reject all those detections that are smaller than the beam area of the observations and less extended in velocity than the spectral broadening. We stress that a three-dimensional source finding algorithm, unlike the two-dimensional methods, can isolate sources with different kinematics even if they are totally or partially overlapped in the plane of the sky. Indeed, if two sources have radial velocities that differ more than the typical velocity resolution ($\sim 10\text{-}15 \text{ km s}^{-1}$), they are always detected as separate sources, no matter whether they overlap or not in the sky.

2.2. Accretion and star formation rate estimates

The main purpose of this study is to estimate the maximum gas accretion rate coming from minor mergers. In the following we describe our assumptions.

Firstly, we assume that all dwarf galaxies will collide in the future with the main galaxies and that their gas will be entirely and instantaneously accreted. Secondly, we assume that the collision will occur in the shortest possible time. In order to calculate this time, we make the satellites moving in parabolic trajectories leading to impact the outer regions of the main galaxies. The orbit is defined in the three-dimensional space by fixing the focus of the parabola at the centre of the main galaxy, imposing the passage through the satellite and fixing the position of the orbital peri-centre at a distance equal to the maximum radius of the central galaxy (Fig. 1). For a generic conic orbit, the time-scale of collision can be obtained by using the equation of the true anomaly ν of celestial mechanics:

$$\int_0^\nu \frac{d\nu'}{(1 - e \cos \nu')^2} = \sqrt{\frac{\mu}{p^3}} (t - T_0) \quad (2)$$

where e is the eccentricity of the orbit, T_0 is the time of the peri-centre passage, p is the semi-latus rectum of the conic section and $\mu = G(M_{\text{main}} + M_{\text{sat}}) \sim GM_{\text{main}}$ is the total dynamical mass of the system galaxy plus satellite multiplied by the gravitational constant G . The dynamical mass of the central galaxy $M_{\text{main}}(R_{\text{max}}) = G^{-1} v_c(R_{\text{max}})^2 R_{\text{max}}$ is calculated within the maximum radius R_{max} of the source, estimated by the searching algorithm. The circular velocity v_c is obtained from the velocity widths of the H I global profiles at the 20% of the peak flux corrected for the inclination taken from the HyperLEDA catalogue. Solving the integral (2) for parabolic orbits ($e = 1$) one obtains the following formula which describes the variation of the true anomaly ν as a function of time:

$$\tan \frac{\nu}{2} + \frac{1}{3} \tan^3 \frac{\nu}{2} = \sqrt{\frac{\mu}{p^3}} (t - T_0) \quad (3)$$

where the semi-latus rectum for parabolic orbit is $p = 2R$, being R the distance between the focus and the vertex of the parabola (Fig. 1).

Using equation (3), we can estimate the time of the peri-centre passage T_0 by calculating ν through a de-projection of the projected anomaly ν_p of the dwarf galaxy measured in the plane of the sky. The accretion rate of cold gas onto a certain galaxy is then obtained by dividing the H I mass of each dwarf by its time of peri-centre passage:

$$\dot{M}_{\text{HI}} = \sum_{i=0}^n M_{\text{HI},i} / T_{0,i} \quad (4)$$

where the sum is taken over all the detected companion galaxies. The H I mass M_{HI} is calculated from the flux density using the following relation (Roberts 1975):

$$M_{\text{HI}} = 2.356 \times 10^5 D^2 \int S(\nu) d\nu \quad (5)$$

where $\int S(\nu) d\nu$ is the integral across the line of the flux density corrected for the primary beam attenuation and expressed in Jy km s^{-1} and D is the distance in Mpc. The equation (5) is valid

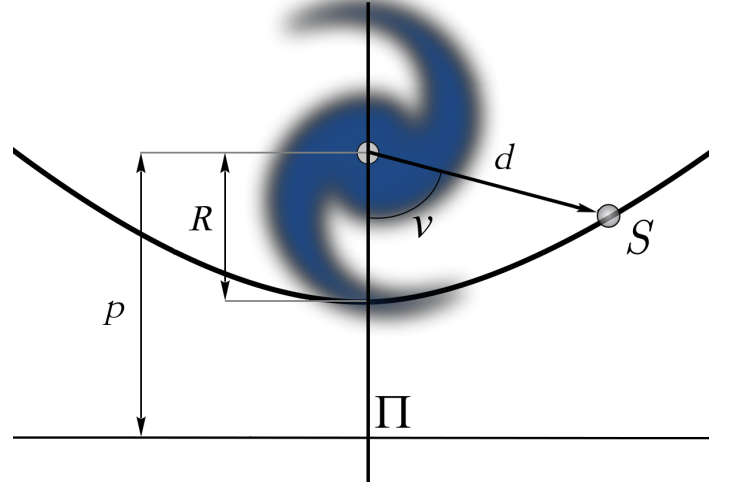


Fig. 1. Schematic view of the parabolic orbit approximation. The blue spiral is the main galaxy, S is the satellite with projected distance d and true anomaly ν . The distance p between the center of the spiral galaxy and the directrix Π of the parabola is two times the outer radius R of the main galaxy R .

under the assumption that the gas is optically thin, which is generally a good approximation for neutral hydrogen, especially in dwarf galaxies, thus no correction for H I self-absorption was applied. The distances were preferably taken from the Extragalactic Distance Database (EDD, Tully et al. 2009), available for a number of galaxies with v_{sys} up to 10000 km s^{-1} and mostly obtained from Cepheids, TRGB, SNIa or Cosmicflows-2 project (Tully et al. 2013). Otherwise, we used the NASA/IPAC Extragalactic Database (NED). For seven galaxies with no available better estimates, we used the Hubble flow $D = v_{\text{sys}}/H_0$ with $H_0 = 70 \text{ km s}^{-1} \text{ Mpc}^{-1}$ and the systemic velocity v_{sys} corrected for Virgo-centric inflow using the values given by the HyperLEDA catalogue.

We compare the total gas accretion (4) to the gas depletion due to the star formation process in the discs. The SFR of the central galaxies was calculated from the far-infrared luminosities (Kennicutt 1998):

$$\text{SFR} = \frac{L_{\text{FIR}}}{2.2 \times 10^{43}} \text{ M}_{\odot} \text{ yr}^{-1} \quad (6)$$

with the L_{FIR} in erg s^{-1} obtained from the far-infrared flux FIR defined after Helou et al. (1985) as:

$$\text{FIR} = 1.26 \times 10^{-11} (2.58 f_{60\mu} + f_{100\mu}) \text{ erg s}^{-1} \text{ cm}^{-2} \quad (7)$$

where $f_{60\mu}$ and $f_{100\mu}$ are the fluxes at 60 and 100 micron expressed in Jansky. In this work we used the IRAS fluxes taken from NED and HyperLEDA. All main galaxies in our sample are detected both at 60μ and 100μ . See Tab. A.1 for their main physical properties.

2.3. Major and minor mergers

We split major and minor mergers depending on the baryonic mass ratio: pair of galaxies with $M_{\text{bar,sat}}/M_{\text{bar,main}} \leq 0.20$ are

classified as minor mergers, otherwise as major. We preferably estimate the baryonic mass as:

$$M_{\text{bar}} = M_* + 1.4M_{\text{HI}} \quad (8)$$

where the factor 1.4 take into account the helium gas fraction. We neglected the contribution of molecular gas. The HI mass M_{HI} is directly estimated from data-cubes through eq. (5). A rough estimate of the stellar mass M_* is obtained by using the total K_s -band magnitude, corrected for extinction, taken from the 2MASS Redshift Survey (2MRS, Huchra et al. 2012) and adopting the following formula (e.g. Longhetti & Saracco 2009):

$$\log_{10}(M_*) = \log_{10}(M/L_K) - 0.4[K + 5 - 5 \log_{10}(D_{[\text{pc}]}) - 3.28] \quad (9)$$

where M/L_K is the stellar mass-to-light ratio (in solar units) in the K-band and 3.28 is the absolute K-band magnitude of the Sun in the Vega system (Binney & Merrifield 1998). We assumed a constant value of mass-to-light ratio $M/L_K = 0.6 M_{\odot}/L_{\odot,K}$, compatible with stellar population models (e.g. Portinari et al. 2004) with a Kroupa IMF (Kroupa 2002).

When 2MRS magnitudes were not available, namely for most dwarf satellites and a few main galaxies, we directly derived M_{bar} from the Baryonic Tully-Fisher Relation (BTFR):

$$\log_{10}(M_{\text{bar}}) = a \log_{10}(v_{\text{flat}}) + b \quad (10)$$

with $a = 3.82 \pm 0.22$ and $b = 2.01 \pm 0.41$ (McGaugh 2012). The v_{flat} was assumed as half of the inclination-corrected velocity widths w_{20} of the HI global profiles at the 20% of the peak flux. Since inclination angles are not known for most dwarf satellites, we adopted an average inclination of 60 degrees for these galaxies.

2.4. The data sample

The Westerbork HI survey of Irregular and Spiral galaxies Project (WHISP, van der Hulst et al. 2001) is a survey of the neutral hydrogen content in galaxies selected from the Uppsala General Catalogue (UGC, Nilson 1973) and observed with the Westerbork Synthesis Radio Telescope (WSRT). WHISP is to date the largest publicly available catalogue of HI nearby galaxies observed with an interferometer and it includes galaxies at $\delta > 20^\circ$ (B1950) with major axis apparent size $> 1.2'$ (B band) and HI flux densities $F_{\text{HI}} > 100$ mJy. Objects satisfying these selection criteria have generally systemic velocities less than 6000 km s^{-1} , i.e., distances lower than 85 Mpc using the Hubble flow with $H_0 = 70 \text{ km s}^{-1} \text{ Mpc}^{-1}$. The galaxies were chosen to be reasonably distributed over all Hubble types, even if later-type galaxies are favoured by the observational criteria. The highest spatial resolution for the WHISP data is $12'' \times 12''/\sin(\delta)$, the typical channel separation is of the order of 5 km s^{-1} . In this work, we used both HI data-cubes spatially smoothed to $30'' \times 30''$ and $60'' \times 60''$. The original sample comprises 256 data-cubes containing about 370 galaxies.¹

Since our goal is to study dwarf satellites around large star-forming galaxies, we selected a sub-sample of spiral galaxies by keeping only those data-cubes containing at least one galaxy

¹ The datacubes, the column density maps and the velocity fields of the WHISP galaxies, at $12''$, $30''$ and $60''$ of resolution, are publicly available for the ‘‘Westerbork on the Web’’ project at ASTRON (<http://www.astron.nl/wow/>).

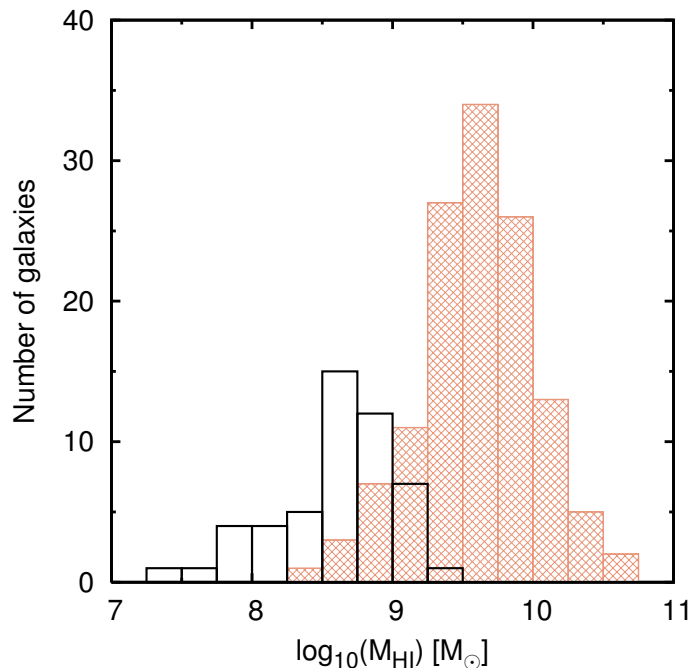


Fig. 2. HI Mass distribution of the detected galaxies in the WHISP sample. Orange shadowed boxes show the spiral galaxies selected as $v_{\text{flat}} > 100 \text{ km s}^{-1}$, black boxes show their dwarf satellites.

with rotation velocity $v_{\text{flat}} = w_{20}/(2 \sin i) > 100 \text{ km s}^{-1}$. The selection was performed through a cross-correlation between the w_{20} estimated directly from the data-cubes and the w_{20} calculated using the Tully-Fisher relation from Sakai et al. (2000):

$$M_B = -(7.97 \pm 0.72)(\log w_{20} - 2.5) - (19.80 \pm 0.11) \quad (11)$$

where M_B is the B-band absolute magnitude (corrected for galactic extinction and k-correction), taken from HyperLEDA. We kept only galaxies for which both methods returned $v_{\text{flat}} > 100 \text{ km s}^{-1}$. This cross-correlation is needed to avoid spurious selections related to some unreliable inclination angles in the HyperLEDA catalogue. Our final sample has 148 data-cubes. Spiral galaxies therein have usually neutral hydrogen masses between $10^9 M_{\odot}$ and few $10^{10} M_{\odot}$ (Fig. 2). The global properties of the main galaxies are listed in Tab. A.1.

3. Results

We ran our code both on data-cubes smoothed to $30''$ and $60''$. The results obtained with these two data sets are thoroughly comparable. We fixed a sigma-clipping threshold for the source finder equal to 4 (see equation 1) and a secondary threshold for growing objects at the edges of 2.5. After extensive experiments, these values appeared the best compromise between reaching low sensitivities and avoiding spurious detections.

We found that, among 148 data-cubes, 101 ($\sim 68.2\%$) had no detectable companions, whereas 47 ($\sim 31.8\%$) contained multiple systems. Among these 47 data-cubes, 15 ($\sim 10.1\%$ of the total, $\sim 31.9\%$ of multiple systems) contained only galaxies with similar masses ($M_{\text{bar,sat}}/M_{\text{bar,main}} > 0.20$). Six data-cubes ($\sim 4.1\%$ of the total, $\sim 12.8\%$ of multiple systems) show both major and minor companions and 26 data-cubes ($\sim 17.6\%$ of the

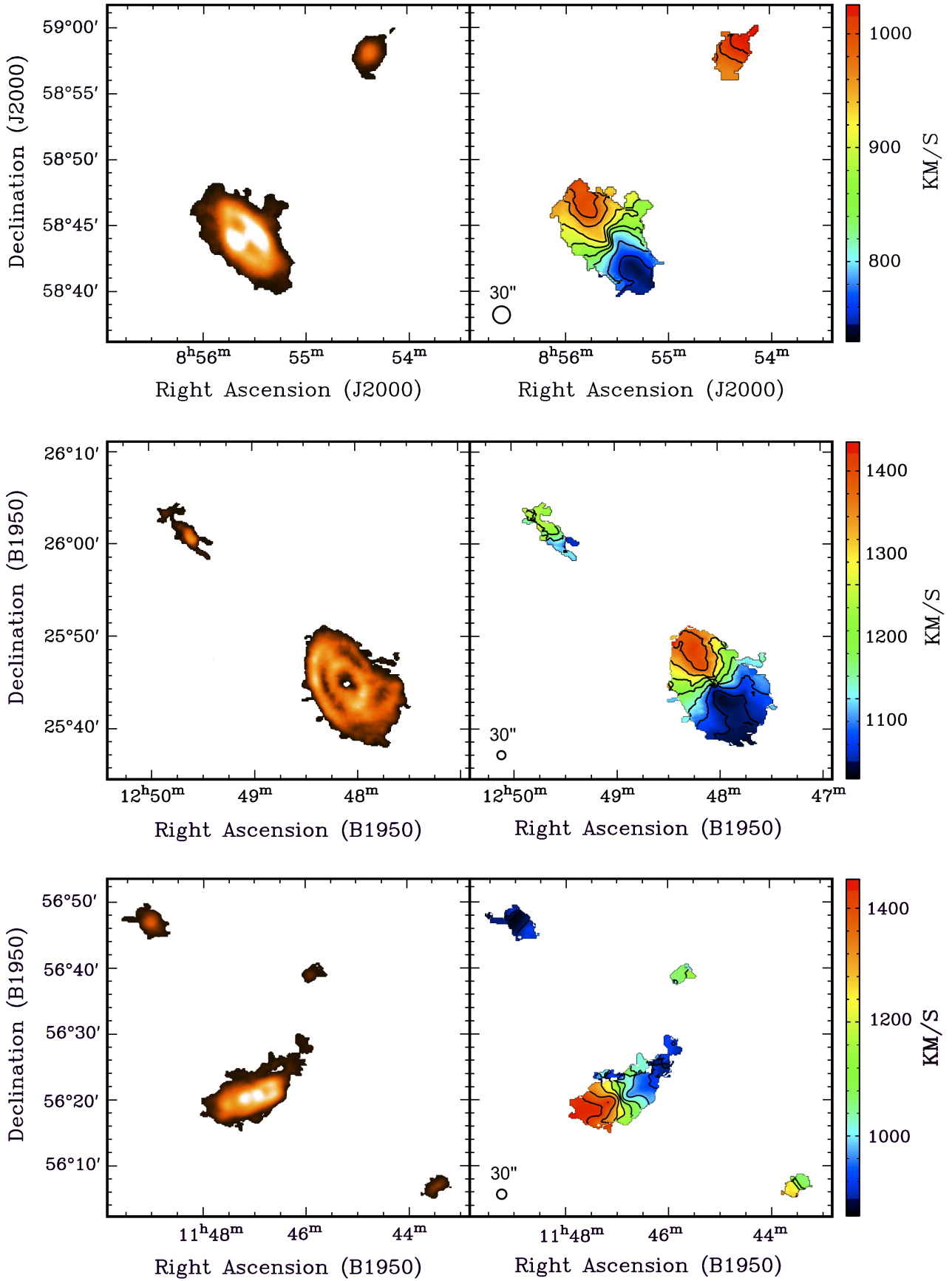


Fig. 3. Three examples of multiple systems in the WHISP sample. From the *top* to the *bottom*, UGC 4666, UGC 7989, UGC 6787 and their dwarf companions. In the *left panels*, the H I column-density maps (0th moment), in the *right panels*, the velocity fields (1st moment) obtained from 30'' smoothed data-cubes.

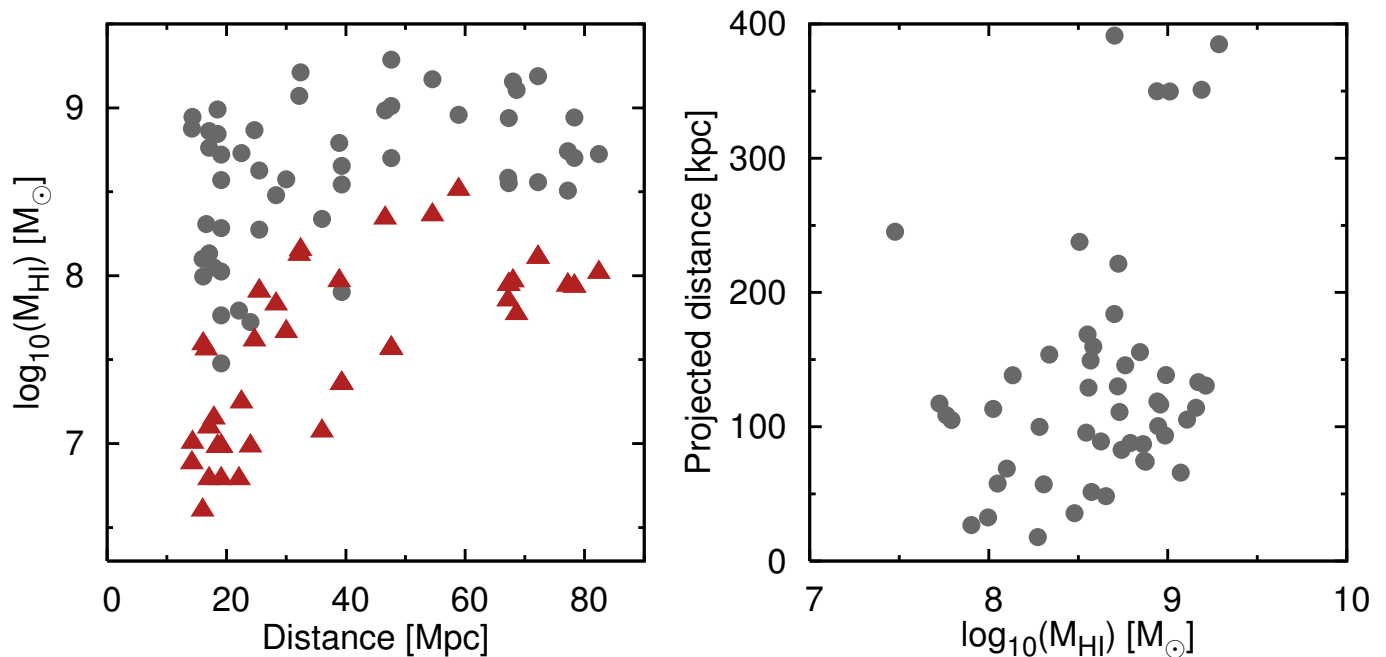


Fig. 4. *Left panel:* the gray dots show the HI masses of detected companions as a function of distance, red triangles are the lowest detectable mass in the correspondent data-cubes. *Right panel:* distance from the main galaxies projected onto the plane of the sky of the detected satellites as a function of their HI mass.

total, $\sim 55.3\%$ of multiple systems) show only dwarf companions. Overall, among 148 analysed data-cubes, 21 ($\sim 14.2\%$), show companions which could be possible candidates for a future major merging, while 32 data-cubes ($\sim 21.6\%$) show potential candidates for minor mergers. Some examples of spiral galaxies with minor satellites are shown in Fig. 3.

We focused on potential minor mergers and all data-cubes with only major companions were excluded from the further analysis. For the six data-cubes with both type of companions, we assumed as the main galaxy the one with the largest HI mass and we ignored the other spiral galaxies. The total number of dwarf gas-rich satellites detected is 50 (Tab. 1). Forty-six dwarf galaxies have a clear optical counterpart in the Sloan Digital Sky Survey (SDSS) or in the Digitized Sky Survey (DSS) images. Four detections, marked with an asterisk in Tab. 1, are not univocally identifiable and they could be either very faint dwarf galaxies or HI clouds. Most satellites are already catalogued in galaxy archives. Ten galaxies, marked with a dagger in Tab. 1, seem not to be catalogued. The HI masses of the detected dwarf galaxies vary between about $10^7 M_{\odot}$ and few $10^9 M_{\odot}$. The HI mass distribution of the main galaxies and their minor satellites is shown in Fig. 2. The mass function for spiral galaxies is peaked at $\log M_{\text{HI}[M_{\odot}]} \sim 9.5$, consistently with studies on wider HI samples (e.g., Zwaan et al. 2005). Most dwarf companions have masses of a few $10^8 M_{\odot}$ and their mass distribution has a cut-off above $5 \times 10^9 M_{\odot}$. This is partially due to our selection criteria. However, it is interesting to note that this distribution is fairly comparable with that of HI-rich dwarf galaxies in the Local Group and in Local Group analogues (e.g., Grcevich & Putman 2009; Pisano et al. 2011). In Fig. 4 we show the HI masses of the detected dwarf galaxies as a function of the distance from the Milky Way. The red triangles represent the minimum detectable mass for each data-cube, calculated using equation (5) on a three-dimensional region with the size of a spatial beam times the velocity resolution (two channels) and a

flux of $4 \times \text{R.M.S.}$ noise of the cube. This is the minimum mass that an object must have to be accepted by the source-finding algorithm. Note the bias effect on the detectable mass due to the distance (see discussion in 4.1).

The projected distances of the dwarf satellites from the main galaxies usually range from some dozen to a few hundred kiloparsecs and typical time-scales for collisions, estimated through the parabolic orbit approximation, are between ~ 100 Myr and 2 Gyr. The number of dwarfs within 100 kpc from the main galaxies and between 100 and 200 kpc is almost the same. In the *right panel* of Fig. 4 we show the projected distance as a function of the dwarf HI masses. Within 200 kpc, dwarf galaxies are quite uniformly distributed over the HI masses. There is a weak tendency for companions to be more massive at larger distances, as we may expect. However, there is an observational bias that can affect this plot. It is a combination of two effects: the linear field-of-view of the observations increases with distance, while the minimum detectable mass (Fig. 4, *left panel*) and the linear resolution decrease. Thus we may detect preferentially companions with lower masses closer to the main galaxies and vice-versa. Moreover, there is also a selection effect due to the primary beam attenuation, i.e. at large angular distances, only massive systems are detected because of the lower sensitivity of the instrument. These effects make it difficult to compare our findings with studies of dwarfs galaxies in the Local Group.

The systemic velocity of dwarf galaxies is calculated as the average midpoint between the velocities at the 20% and 50% of the peak flux of their global HI profiles. The $\Delta v_{\text{sys}} = \|v_{\text{sys,main}} - v_{\text{sys,sat}}\|$ ranges between a few tens to a few hundreds km s^{-1} . Satellites do not have systemic velocities that differ more than 300 km s^{-1} from those of the main galaxies. The velocity widths w_{20} of dwarf galaxies, taken at the 20% of the peak flux, are usually lower than 200 km s^{-1} , even if corrected for a mean inclination of 60 degrees, except for three galaxies. Overall, most of the satellites have $w_{20} < 100 \text{ km s}^{-1}$.

Table 1. Detected companions of the WHISP spiral galaxies with $M_{\text{bar,sat}}/M_{\text{bar,main}} \leq 0.20$: (1) First name in NED archive or DF if not classified, (2) UGC name of the main galaxy, (3) celestial coordinates, (4) adopted distance [same as the main galaxy or taken from EDD catalogue, when specified], (5) systemic velocity, (6) line width of the global profile at the 20% level, (6) total HI mass, (8) projected distance from the main galaxy (9) time of collision with the main galaxy in a parabolic orbit, (10) gas accretion rate onto the main galaxy.

Name	Main galaxy	Coord. (J2000)	D	v_{sys}	w_{20}	M_{HI}	d_{proj}	t_{coll}	\dot{M}_{HI}
(1)	(2)	RA-Dec	Mpc	km/s	km/s	$10^8 M_{\odot}$	kpc	10^8 yr	M_{\odot}/yr
		(3)	(4)	(5)	(6)	(7)	(8)	(9)	(10)
AGC 102802	UGC 485	J004702.7+301243	58.9	5296	85	9.08	117	15.7	0.58
AGC 113996	UGC 624	J010107.2+304052	78.3	4762	29	8.76	119	11.6	0.75
AGC 113884	UGC 624	J010000.3+302357	78.3	4717	96	5.04	391	17.8	0.28
[VH2008] J0101+4744	UGC 625	J010118.4+474432	28.3	2795	62	3.02	36	4.5	0.67
DF1 [†]	UGC 1437	J015708.1+354825	54.5	4592	172	14.80	133	9.8	1.51
PGC 9994	UGC 2141	J030653.0+301542	24.7	812	43	7.37	75	5.6	1.32
PGC 2328690	UGC 2459	J030225.7+485452	32.4	2449	134	16.29	131	14.3	1.14
[KLT2208] HI J0302+352*	UGC 2487	J030210.5+351627	72.2	4933	55	15.43	351	18.1	0.85
[SOS2010] J0301491+3529012	UGC 2487	J030147.2+352839	72.2	4876	38	3.61	129	8.6	0.42
UGC2813	UGC 2800	J034234.1+711828	16.1 ¹	1381	62	0.99	33	4.2	0.24
HFLZOA G136.96+14.21	UGC 2916	J040403.5+713707	68.0	4450	158	14.36	114	10.8	1.33
2MASX J04550438+3002212	UGC 3205	J045826.3+295653	47.6	3239	173	10.26	350	17.6	0.58
DF2 [†]	UGC 3205	J045504.2+300209	47.6	3530	47	5.03	184	9.7	0.52
DF3 [†]	UGC 3205	J045653.8+293602	47.6	3229	110	19.34	385	18.3	1.06
DF4 [†]	UGC 3382	J055903.3+621719	67.2	4407	64	3.83	160	12.6	0.30
DF5 [†]	UGC 3407	J060841.0+415647	39.3	3683	66	3.50	96	10.1	0.35
DF6 [†]	UGC 3407	J060913.3+420104	39.3	3688	114	4.51	48	7.9	0.57
DF7 [†]	UGC 3407	J060853.9+420338	39.3	3693	73	0.80	27	3.5	0.23
DF8 ^{†*}	UGC 3422	J061633.1+705743	77.2	4009	24	3.22	238	9.8	0.33
GALEXASC J061256.68+710650.6	UGC 3422	J061254.8+710659	77.2	3998	104	5.52	83	7.5	0.74
NPM1G +60.0018	UGC 3546	J065150.2+604122	17.9	1768	52	1.12	58	5.8	0.19
GALEXASC J070643.91+635521.0	UGC 3642	J070645.1+635515	67.3	4714	106	3.56	169	11.1	0.32
UGC 3660	UGC 3642	J070634.1+635056	67.3	4261	75	8.70	350	17.9	0.49
KUG 0829+227B	UGC 4458	J083247.7+223443	68.6	4621	231	12.80	105	12.4	1.03
MCG +10-13-030	UGC 4666	J085422.1+585908	16.0	1016	90	1.26	69	5.7	0.22
SDSS J091001.72+325659.8	UGC 4806	J091005.0+325607	25.5	2049	125	4.23	89	9.5	0.45
KUG 0906+333A	UGC 4806	J090919.5+330734	25.5	1897	60	1.88	18	5.7	0.33
SDSS J093137.13+292533.3	UGC 5060	J093138.0+292534	24.0	1608	77	0.53	117	9.9	0.05
KDG 059	UGC 5253	J095156.6+720439	16.6	1121	46	2.03	57	6.2	0.33
UGC 6797	UGC 6778	J114940.5+482533	17.1	962	81	7.28	87	8.5	0.86
SDSS J115027.42+490105.9	UGC 6778	J115027.4+490106	17.1	1120	31	1.67	138	11.2	0.12
UGC 6791	UGC 6786	J114923.6+264428	22.5 ¹	1866	274	5.38	111	10.0	0.54
SDSS J114820.16+562045.7	UGC 6787	J114820.6+562049	22.1	1080	28	0.62	105	7.6	0.08
UGC 6733	UGC 6787	J114535.7+555313	19.1 ²	1158	187	5.26	130	10.3	0.51
UGC 6816	UGC 6787	J115047.5+562719	17.1 ¹	887	115	5.78	146	11.0	0.52
SDSS J122442.59+544441.3	UGC 7506	J122440.2+544448	36.0	2495	109	2.18	154	11.6	0.19
UGC 8005	UGC 7989	J125149.1+254644	14.3 ¹	1196	198	8.84	101	8.6	1.02
UGC 8254	UGC 8307	J131038.2+363807	19.1	1088	105	3.71	149	16.1	0.23
DF9 ^{†*}	UGC 8307	J131153.6+362758	19.1 ¹	954	75	1.92	100	14.2	0.14
UGC 8271	UGC 8307	J131131.3+361655	18.5 ¹	1145	150	6.99	156	22.1	0.32
DF10 ^{†*}	UGC 8307	J131134.3+362942	19.1	1191	32	0.58	109	15.5	0.04
KUG 1309+362	UGC 8307	J131146.7+355731	19.1	1123	26	0.30	245	24.9	0.01
UGC 8303	UGC 8307	J131317.6+361303	18.5 ¹	948	92	9.77	139	20.3	0.48
UGC 8314	UGC 8307	J131401.0+361908	19.1	938	71	1.06	113	21.2	0.05
MCG +08-27-001	UGC 9366	J143359.2+492647	38.9	2122	127	6.18	88	6.2	1.00
KUG 1512+557	UGC 9797	J151400.2+553222	46.6	3550	154	9.66	94	9.4	1.03
SDSS J152617.51+404004.0	UGC 9858	J152617.9+404008	32.2	2687	51	11.80	66	7.7	1.53
MCG +08-34-005	UGC 11283	J183400.4+492233	30.0	2076	63	3.75	51	7.5	0.50
GALEXASC J215645.61+275419.5	UGC 11852	J215645.7+275418	82.4	5710	46	5.30	221	15.2	0.35
ZOAG G095.92-08.72	UGC 11951	J221145.4+453649	14.2	1145	78	7.52	74	8.3	0.91

[†] Not catalogued in the NED, HyperLEDA or SIMBAD archives.

* Without a clear optical/UV counterpart in DSS, SDSS or GALEX images. DF8 is not covered by the SDSS survey.

¹ Distance from EDD catalogue.

For each data-cube with identified dwarf companions, we calculated the maximum possible accretion rate of cold hydrogen gas \dot{M}_{HI} onto the main galaxy, the star formation rate \dot{M}_{SF} of the main galaxy and the ratio $\dot{M}_{\text{HI}}/\dot{M}_{\text{SF}}$. For all galaxies, with or without identified companions, a potentially hidden accretion from dwarfs below the detectability limit was

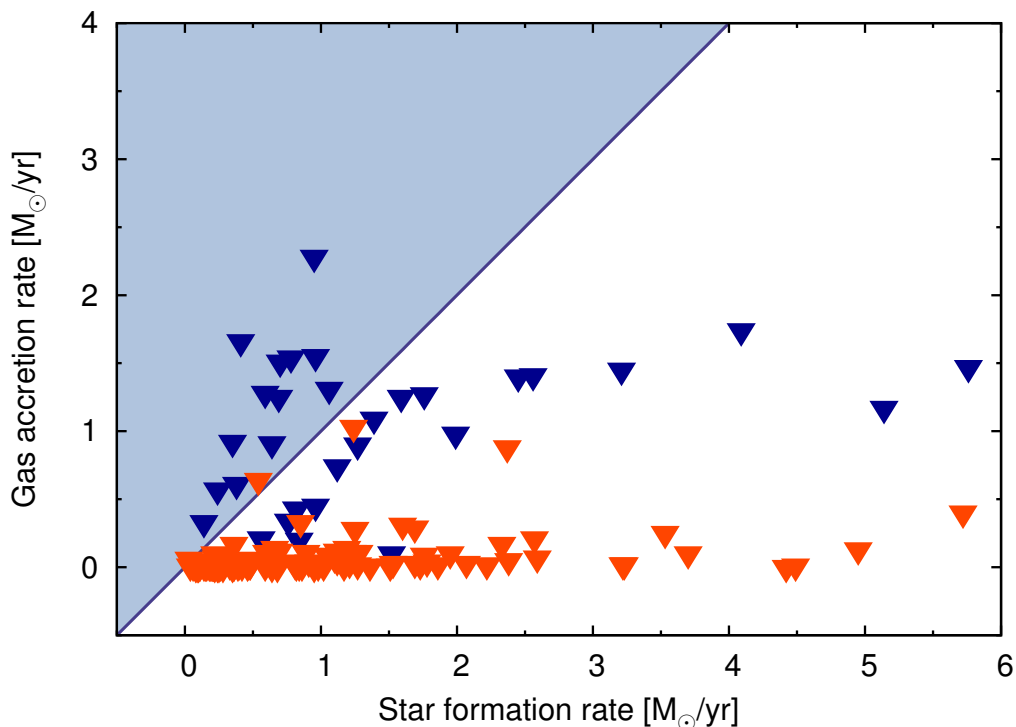


Fig. 5. Upper limits to the cold gas accretion rates from satellites vs star formation rates in spiral galaxies in the WHISP sample. The inverted dark blue triangles are upper limits to the gas accretion rate for galaxies with detected satellites (including both visible and hidden accretion), the inverted orange triangles are the hidden accretion upper limits for galaxies without companions, estimated as discussed in the text. The star formation rates are lower limits calculated from the far-infrared fluxes. The blue-shadowed region represents a complete feeding of SF through minor mergers.

estimated. The hidden accretion rate was calculated by dividing the above-mentioned minimum detectable mass by the average collision time over the sample, i.e. 1.1 Gyr. Integrating the HI mass function ($\phi_* [\text{Mpc}^{-3} \text{dex}^{-1} h_0^3] = 4.8 \pm 0.3 \times 10^3$, $\log(M_*/M_\odot) + 2 \log h_0 = 9.96 \pm 0.02$ and $\alpha = -1.33 \pm 0.02$, (Martin et al 2010)) below the detection limit and within the volume of each data-cube always gives HI masses lower than minimum detectable mass. Thus, with our choice we are maximizing the mass of the undetected galaxies.

We found a mean upper limit for the accretion in galaxies with identified minor companions of $0.86 \text{ M}_\odot \text{ yr}^{-1}$, with a mean ratio $\langle \dot{M}_{\text{HI}}/\dot{M}_{\text{SF}} \rangle \sim 0.67$. A more meaningful estimate is however the mean upper limit to the accretion over the whole sample, that turns out to be $\dot{M}_{\text{HI}} = 0.28 \text{ M}_\odot \text{ yr}^{-1}$ against the average star formation rate of $1.29 \text{ M}_\odot \text{ yr}^{-1}$, with a mean ratio $\langle \dot{M}_{\text{HI}}/\dot{M}_{\text{SF}} \rangle \sim 0.22$. The median of $\dot{M}_{\text{HI}}/\dot{M}_{\text{SF}}$ is 0.07. Thus, the ratio of the gas needed for star formation to the maximum gas accretion provided by minor mergers is between 5 and 14. Considering a fraction of gas recycle from stellar feedback of 30% (e.g. Naab & Ostriker 2006) leads to a ratio between 3 and 10.

The above results show that the number of dwarf galaxies in the Local Universe is on the average too low to guarantee the continuous gas replenishment needed by star formation. In Fig. 5 we show a plot of \dot{M}_{HI} versus \dot{M}_{SF} for each galaxy individually. If the gas accretion were large enough to sustain the star formation of the main galaxies, the data points would have fully populated the blue-shadowed region in the upper-left corner, whereas the vast majority lie well below the blue straight-line indicating a ratio $\dot{M}_{\text{HI}}/\dot{M}_{\text{SF}} = 1$. We conclude that minor mergers can not bring enough gas to the discs and sustain star formation. Once again,

our values of gas accretion rates are very strong upper limits, because of our very stringent assumptions, and the real accretion rates could reasonably be one order of magnitude lower than our estimate. Incidentally, we note that our assumptions would imply that all dwarf galaxies disappear in the next 2 Gyr. We stress that our SFRs are likely lower limits as they are calculated using only FIR fluxes. This bias goes in the direction of strengthening our findings.

We repeated the analysis of the WHISP data-cubes using a sigma-clipping threshold for the sources of 3σ and 5σ . Reducing the detection threshold leads the program to identify many more dwarf companions: more than 100 minor satellites are detected at the lower level, but most of these sources are clearly false detections and the results obtained would be very likely unreliable. Such a large fraction of wrong detections is probably due to the low signal-to-noise of the WHISP data-cubes. Instead, increasing the detection threshold to 5σ leads to results very similar to those described above as just two of the dwarf companions found at 4σ are missed by the rejection criteria, namely the satellites of UGC 7506 and UGC 9858. These companions are actually good detections, as quoted in the literature (Noordermeer et al. 2005), but at a 5σ level they are discarded by the one beam covering requirement. The mean values of the accretion rate at 5σ are also in agreement with those found at 4σ .

4. Discussion

The application of our code to the WHISP catalogue led to a firm upper limit for the accretion of cold gas from minor mergers in the Local Universe of $0.28 \text{ M}_\odot \text{ yr}^{-1}$. The total multiple system

fraction for the WHISP sample is $\sim 32\%$, in particular $\sim 22\%$ of galaxies are accompanied by minor companions and $\sim 14\%$ are major systems. Here we discuss the main uncertainties of our results and their relevance.

4.1. Uncertainties

Our estimate does not take into account the molecular fraction. The amount of molecular gas in dwarf galaxies is highly unconstrained as they are often undetected in CO emission lines (e.g., Taylor et al. 1998). They also usually have low metallicities, making the conversion between CO and H_2 even more uncertain (e.g., Boselli et al. 2002). However, any realistic correction for molecular gas should not increase our accretion rate by more than a factor two.

WHISP is a source-targeted survey and it can not be obviously considered as a complete sample. The selection criterion, grounded on the apparent size of the observed galaxies, produces a catalogue that favours progressively larger and more massive galaxies moving to greater distances from the Milky Way. This effect can be appreciated in Fig. 4 (upper envelop) although it appears to be not too severe. The growth with the distance of the minimum detectable mass furthermore makes it impossible to detect low mass satellites at large distances. In order to test the importance of these biases, we have considered only those data-cubes with a minimum detectable mass $M_{\text{det}} \leq 10^8 M_{\odot}$. In this way, we can obtain a sub-sample of galaxies where satellites are quite uniformly distributed over the mass and the distance ranges (left panel of Fig. 4). The maximum accretion rate obtained in this case is $0.21 M_{\odot} \text{ yr}^{-1}$. Reducing the threshold to data-cubes with $\log M_{\text{det}} \leq 5 \times 10^7 M_{\odot}$ leads to a maximum accretion rate of $0.18 M_{\odot} \text{ yr}^{-1}$. These values indicate that our accretion rate estimates is not strongly affected by the incompleteness of the sample of the dwarf galaxies.

Another bias effect is related to the linear field of view, which is greater at larger distances. In the farthest systems, the field of view allows us to observe satellites with projected distances of some hundreds kpc from the main galaxies, whereas we can not go beyond one hundred kpc in the closest systems. The primary beam attenuation of the WSRT is significantly large ($\sim 80\%$ of the flux is missed) beyond $25'$ from the pointing center, corresponding to ~ 70 kpc at about 10 Mpc. This indicates that we should be able to detect fairly separated satellites also in the nearest systems. The most distant satellites have larger collision time-scales and their contribution to the global accretion is expected to be smaller. In our sample, considering only satellites within 100 kpc from the main galaxies gives an accretion rate of $0.38 M_{\odot} \text{ yr}^{-1}$, $0.27 M_{\odot} \text{ yr}^{-1}$ between 100 and 200 kpc and $0.21 M_{\odot} \text{ yr}^{-1}$ beyond 200 kpc (the global value being $0.86 M_{\odot} \text{ yr}^{-1}$). These results show that the contribution of very distant satellites is progressively less important, thus the limited field of view of the closest systems should not significantly affect our accretion rate estimate.

In the literature, mergers are usually classified on the basis of their dynamical mass ratio: pair of galaxies with $M_{\text{sat}}/M_{\text{main}} \leq 0.1 - 0.2$ are considered minor mergers, otherwise major mergers. Unfortunately, we can not trivially estimate the dynamical masses of satellite galaxies from the H I data. Thus, in this work, we divided satellites depending on the ratio of their baryonic mass to the main galaxy baryonic mass. Satellites with baryonic content lower than 20% of the main galaxies ($M_{\text{bar,sat}}/M_{\text{bar,main}} \leq 0.20$) are classified as minor companions. This is an arbitrary but conservative choice, since most detected satellites have mass ratio $\ll 0.05$. It is however interesting to quantify the accre-

tion rate using different baryonic mass ratios. In our sample, the maximum accretion rate ranges between $0.20 M_{\odot} \text{ yr}^{-1}$ for $M_{\text{bar,s}}/M_{\text{bar,g}} \leq 0.1$ and $0.56 M_{\odot} \text{ yr}^{-1}$ for $M_{\text{bar,sat}}/M_{\text{bar,main}} \leq 0.5$. If we consider the whole galaxy pairs as potential mergers and we calculate the accretion rate by accreting the less massive ones onto the most massive ones, we obtain the value of $1.22 M_{\odot} \text{ yr}^{-1}$. Even such an excessive overestimate turns out to be of the same order of the mean SFR. We conclude that mergers in the Local Universe can not sustain the star formation in spiral galaxies.

4.2. Comparison to other estimates

The accretion of cold gas from minor mergers in the Local Universe has been estimated by Sancisi et al. (2008), visually inspecting and comparing total maps, velocity fields and position-velocity diagrams for the WHISP galaxies. They found a minor merger fraction of about 25%. Unlike our approach, they considered only those systems that show clear signs of tidal interactions, such as tails, bridges, disturbed H I morphologies and/or kinematics. Assuming typical H I masses of the dwarfs of the order $10^{8-9} M_{\odot}$ and a lifetime for observed features of about 1 Gyr, Sancisi et al. inferred a mean accretion rate of H I gas around $0.1 - 0.2 M_{\odot} \text{ yr}^{-1}$ and they stressed that such a value is likely a lower limit. It is worth noting that most systems we considered as potential minor mergers were not recognized that way by Sancisi et al. and, on the contrary, many interactions they identified were not found by our code. The reason is simple: our code looks for “separated” objects and it handles all dwarf companions as candidates for minor mergers, also those showing no signs of ongoing interaction. In other words, we look at the population of dwarfs in the environment of a spiral galaxy that could become a minor merger in the next future. Our code identifies companions until the two galaxies start “touching” each other and we estimate the accretion rate using the time-scale for collision as accretion time. Instead, Sancisi et al. (2008) find a later stage of merging, i.e., when galaxies are strongly interacting and the gas is visibly disturbed in the morphology and/or in the kinematics. Consequently, they calculate the accretion rate using as time-scale the dynamical time that it should take for these features to disappear as the gas redistributes uniformly in the disc. In our work the accretion process ends when galaxies touch each other, whereas for Sancisi et al. (2008) that is the starting point. However, since the population of dwarf galaxies has likely remained similar in the last Gyr or so, the two accretion rates should be comparable. Interestingly, our upper limit of $M_{\text{HI}} < 0.28 M_{\odot} \text{ yr}^{-1}$ is not in contradiction with the average accretion rate estimated by Sancisi et al. (2008).

4.3. Merger fraction

Most of recently published studies on the local merging systems have been made using images from optical-UV galaxy surveys (e.g., Patton et al. 2000; Lambas et al. 2012; Robotham et al. 2012) such as the Second Redshift Survey of Southern Sky (SRSS2), the Sloan Digital Sky Survey (SDSS) and the recent Galaxy And Mass Assembly (GAMA) survey, whereas just a couple of studies have been carried on using H I data (Sancisi et al. 2008; Holwerda et al. 2011). These studies have mainly investigated the fraction and the rate (fraction of mergers per comoving volume and time units) of galaxies showing signs of interactions and their evolution with time.

To date, two main approaches have been used to estimate the galaxy merger fraction and both make use of high resolution

imaging. The pair method consists in counting the galaxies spatially separated from each other by less than a few tens of kpc and with spectroscopic radial velocities that do not differ by more than a few hundreds of km s^{-1} (e.g., Le Fèvre et al. 2000; Lin et al. 2008). Using this kind of approach it is possible to estimate a “progenitor galaxy” merger fraction. The second approach identifies mergers by quantifying morphological signatures that can be related to past or ongoing interactions, such as asymmetries and/or tails. This method makes use of several parameters for describing peculiar light distributions, such as the Concentration-Asymmetry-Smoothness parameters (CAS, Conselice 2003) or the Gini- M_{20} parameters (Lotz et al. 2004). This technique can identify mergers in a relatively late stage, but not all asymmetric galaxies are necessary merger features. The asymmetry method is similar to the technique used by Sancisi et al. (2008), whereas our approach on H I data-cubes is conceptually similar to the close pair method. The main difference is that we do not impose any limit for the projected distance between galaxies, whereas the velocity criterion is implicit in the data-cubes. Moreover, we select objects in 3D space (so potentially also overlapping in the sky) and we estimate the minimum time of collision for each galaxy independently.

The asymmetry and close pairs methods have been widely used with optical galaxy surveys, but, despite the large number of studies, there is little consensus on the galaxy merger rate and its evolution with redshift. Current observations of the fraction of galaxy undergoing a merger differ by an order of magnitude, from $\sim 2\%$ (e.g., Patton et al. 2000; De Propriis et al. 2007, 2.3% and 1.9%, respectively) to 15% (e.g., de Ravel et al. 2009) and its trend with redshift vary from no evolution (e.g., Jogee et al. 2009) to strong evolution (e.g., López-Sanjuan et al. 2009). These discrepancies mainly arise from the different criteria for galaxy counting, merger selection and bias in the galaxy samples. The value we found ($\sim 32\%$) is a companion fraction rather than a merger fraction as some companions that we considered are fairly far away from the main galaxies (Fig. 4, *right panel*). It is therefore difficult to compare our fraction with the above mentioned values. Broadly speaking, our estimate, which is indeed an upper limit, is higher at least of a factor 2-3 because our program treats all multiple systems as mergers and, working with H I data, identifies more easily dwarf gas-rich companions compared to optical observations. However, if we exclude the very far away companions, namely those beyond 100 kpc of projected distance, we obtain a companion fraction of $\sim 14\%$, not too different from the values found with optical studies. Finally, we stress that the WHISP sample is insignificant compared to other local references based on large catalogues, such as the SDSS or the Millennium Galaxy Catalogue (MGC), so that our values are less reliable from a statistical point of view.

A recent study carried out by Holwerda et al. (2011) estimated the merger fraction and rate for the whole WHISP sample using both close pair and asymmetry methods on H I total maps. Holwerda et al. found a merger fraction of 7% based on pairs, and 13% based on disturbed morphology. We can not compare our merger fraction with the latter value, because our program ignores the galaxy morphology, but the former value is fully comparable and our estimate is significantly higher by about a factor 4. A possible reason of such a discrepancy is that Holwerda et al. based their pair fraction on 24 multiple systems previously identified and classified as interacting by Noordermeer et al. (2005b) and Swaters et al. (2002b), whereas our code detected a much larger number of satellites (see Tab. 1). If we use this sub-sample, the merger fractions become closely comparable.

4.4. Other channels for gas accretion

How star-forming galaxies can sustain their star formation is still an open question. In this study, we demonstrated that gas-rich minor mergers do not play a primary role and other dominant accretion channels must be admitted. A way to fill the discrepancy between the estimated accretion rates and the SFRs could be to assume that the H I mass function were much steeper in the recent past than now, so that the number of dwarf satellites to be accreted were much higher. However, to date no observational evidence in that direction can be achieved with the present generation of radio-telescopes and studies of the Damped Lyman α systems show a remarkable constancy of the H I mass throughout the Hubble time (e.g., Prochaska & Wolfe 2009). Another possibility is that the most accretion is supported by infalling of gas clouds with H I masses of $10^7 - 10^6 M_{\odot}$, but recent deep observations of nearby groups of galaxies (e.g., Pisano et al. 2007; Chynoweth et al. 2009), as well as large blind surveys, such as ALFALFA (Giovanelli et al. 2007), showed no evidence for a significant population of these small H I clouds. Moreover, studies on the Milky Way’s High Velocity Clouds (HVCs) estimated a contribution to the total gas accretion of $0.1 - 0.2 M_{\odot} \text{ yr}^{-1}$ (e.g., Wakker et al. 2007; Putman et al. 2012), a value much smaller than the SFR. In addition, the gas in the ionized phase could produce a further accretion rate of $\sim 1 M_{\odot} \text{ yr}^{-1}$ (e.g., Shull et al. 2009), but it is not understood whether this gas can feed the star formation process in the disc. Numerical simulations (e.g., Fernández et al. 2012) support the idea that the most of the gas infall in Milky Way-like galaxies is continuously provided by a drizzle and filamentary cosmological accretion, which would be almost undetectable or very difficult to identify (e.g., Lehner et al. 2013; Tumlinson et al. 2013). Finally, large amounts of matter could be supplied by the coronal gas cooling potentially triggered by supernova feedback (Marinacci et al. 2010).

5. Conclusions and future prospects

In this paper, we estimated the maximum accretion of cold gas from minor mergers in a sample of large spiral galaxies from the WHISP catalogue. We used an algorithm of source finding to detect dwarf H I-rich satellites around these spiral galaxies and we assumed that they will disappear and merge with the main galaxies in the shortest possible time. We found that $\sim 22\%$ of galaxies have detected dwarf companions ($M_{\text{bar,sat}}/M_{\text{bar,main}} \leq 0.20$) and we estimated a maximum gas accretion rate onto the main galaxies over the whole sample of $0.28 M_{\odot} \text{ yr}^{-1}$. Given the assumptions, this value is a strong overestimate and the actual value can easily be an order of magnitude or more lower. From far-infrared luminosities, we calculated a mean star formation rate of $1.29 M_{\odot} \text{ yr}^{-1}$, a value which is nearly five times higher than the maximum gas accretion rate. These results strongly suggest that minor mergers can not bring enough gas to guarantee a long lasting star formation process in the discs of the spiral galaxies. We note that our method can also detect, if present, large floating H I clouds and include them in the accretion budget. We did not find any significant population of these clouds. Thus, most of gas accretion seems to be hidden to the current investigations in H I emission.

WHISP is a fairly large sample of nearby galaxies, but it is very small compared to surveys carried out at other wavelengths. The new generation of radio telescopes, such as the SKA (Carilli & Rawlings 2004) and its pathfinders, ASKAP (Johnston et al. 2008) and MeerKAT (Booth et al. 2009) and the restyling of existing interferometers, such as the WSRT with the APERTIF

system (Verheijen et al. 2008) and the Karl G. Jansky VLA, will largely increase the number of available data samples. In the next future, already scheduled HI surveys, such as WALLABY and DINGO with ASKAP, LADUMA with MeerKAT and WNSHS with WSRT/APERTIF, will increase the number of galaxies observed with radio interferometers by three orders of magnitude, from a few hundreds to about 10^5 . It will be very interesting to apply the kind of analysis performed in this paper to those large galaxy samples.

Acknowledgements. We thank Renzo Sancisi, Tom Oosterloo, Thijs van der Hulst and Micol Bolzanella for helpful suggestions and fruitful discussions. EdT personally thanks Gabriele Pezzulli for his daily help and useful advices. We used the WHISP data sample and the EDD, NED, HyperLEDA and Simbad catalogues. This research made use of some parts of the Duchamp code, produced at the Australia Telescope National Facility, CSIRO, by Matthew Whiting. We acknowledge financial support from PRIN MIUR 2010–2011, project ‘The Chemical and Dynamical Evolution of the Milky Way and Local Group Galaxies’, prot. 2010LY5N2T.

References

- Aumer, M., & Binney, J. J. 2009, MNRAS, 397, 1286
 Bell, E. F., McIntosh, D. H., Katz, N., & Weinberg, M. D. 2003, ApJS, 149, 289
 Bertone, S., & Conselice, C. J. 2009, MNRAS, 396, 2345
 Bigiel, F., Leroy, A., Walter, F., et al. 2011, ApJ, 730, L13
 Binney, J., & Merrifield, M. 1998, Galactic Astronomy, Princeton University Press, Princeton NJ
 Bond, J. R., Cole, S., Efstathiou, G., & Kaiser, N. 1991, ApJ, 379, 440
 Boselli, A., Lequeux, J., & Gavazzi, G. 2002, A&A, 384, 33
 Booth, R. S., de Blok, W. J. G., Jonas, J. L., & Fanaroff, B. 2009, ArXiv e-prints/0910.2935
 Bregman, J. N. 2007, ARA&A, 45, 221
 Naab, T., & Ostriker, J. P. 2006, MNRAS, 366, 899
 Carilli, C. L., Rawlings, S. 2004, New A. Rev., 48, 979
 Chiappini, C., Matteucci, F., & Gratton, R. 1997, ApJ, 477, 765
 Chomiuk, L., & Povich, M. S. 2011, AJ, 142, 197
 Chynoweth, K. M., Langston, G. I., Holley-Bockelmann, K., & Lockman, F. J. 2009, AJ, 138, 287
 Conselice, C. J. 2003, ApJS, 147, 1
 Dekel, A., & Birnboim, Y. 2006, MNRAS, 368, 2
 De Propriis, R., Conselice, C. J., Liske, J., et al. 2007, ApJ, 666, 212
 de Ravel, L., Le Fèvre, O., Tresse, L., et al. 2009, A&A, 498, 379
 Fernández, X., Jong, M. R., & Putman, M. E. 2012, ApJ, 749, 181
 Fraternali, F., van Moorsel, G., Sancisi, R., & Oosterloo, T. 2002, AJ, 123, 3124
 Fraternali, F., & Binney, J. J. 2008 MNRAS, 386, 935
 Fraternali, F. 2010, AIPC, 1240, 135
 Fraternali, F., & Tomassetti, M. 2012, MNRAS, 426, 2166
 Grevech, J., & Putman, M. E. 2009, ApJ, 696, 385
 Joge, S., Miller, S. H., Penner, K., et al. 2009, ApJ, 697, 197
 Johnston, S., Taylor, R., Bailes, M., et al. 2008, Exp. Astron., 22, 151
 Kazantzidis, S., Zentner, A. R., Kravtsov, A. V., Bullock, J. S., & Debattista, V. P. 2009, ApJ, 700, 1896
 Kennicutt, R. C. 1998, ApJ, 498, 541
 Kereš, D., Katz, N., Fardal, M., Davé, R., & Weinberg, D.H. 2009, MNRAS, 395, 160
 Giovanelli, R., Haynes, M. P., Kent, B. R., et al. 2007, AJ, 133, 2569
 Heald, G., Józsa, G., Serra, P., et al. 2011, A&A, 526, A118
 Helou, G., Soifer, B. T., & Rowan-Robinson, M. 1985, ApJ, 298, L7
 Hess, K. M., Pisano, D. J., Wilcots, E. M., & Chengalur, J. N. 2009, ApJ, 699, 76
 Holwerda, B. W., Pirzkal, N., de Blok, W. J. G., et al. 2011, MNRAS, 416, 2437
 Hopkins, A. M., McClure-Griffiths, N. M., & Gaensler, B. M. 2008, ApJ, 628, L13
 Hopkins, P. F., Croton, D., Bundy, K., et al. 2010, ApJ, 724, 915
 Huchra, J. P., Macri, L. M., Masters, K. L., et al., 2012, ApJS, 199, 26
 Lacey, C., & Cole, S. 1993, MNRAS, 262, 627
 Kroupa, P. 2002, Science, 295, 82
 Lambas, D. G., Alonso, S., Mesa, V., & O’Mill, A. L. 2012, A&A, 539, A45
 Le Fèvre, O., Abraham, R., Lilly, S. J., et al. 2000, MNRAS, 311, 565
 Lehner, N., Howk, J. C., Tripp, T. M., et al. 2013, ApJ, 770, 138
 Leroy, A. K., Walter, F., Brinks, E., et al. 2008, ApJ, 136, 2782
 Lin, L., Patton, D. R., Koo, David C., et al. 2008, ApJ, 681, 232
 Longhetti, M. & Saracco, P. 2009, MNRAS, 394, 774
 López-Sanjuan, C., Balcells, M., & Pérez-González, P. G. 2009, A&A, 501, 505L
 Lotz, J. M., Primack, J., & Madau, P. 2004, AJ, 128, 163
 Lotz, J. M., Davis, M., Faber, S. M., et al., 2008, ApJ, 672, 177
 Lutz R. K. 1980, The Computer Journal, 23, 262
 Martin, A. M., Papastergis, E., Giovanelli, R., et al. 2010, ApJ, 723, 1359
 McGaugh, S. S. 2012, AJ, 143, 40
 Nilson, P., Uppsala General Catalogue of Galaxies, Acta Universitatis Upsalien-sis, Uppsala Astronomiska Observatoriums Annaler
 Noeske, K. G., Faber, S. M., Weiner, B. J., et al. 2007, ApJ, 660, L47
 Noordermeer, E., van der Hulst, J. M., Sancisi, R., Swaters, R. A., & van Albada T. S. 2005b, A&A, 442, 137
 Marinacci, F., Binney, J. J., Fraternali, F., Nipoti, C., Ciotti, L., & Londrillo, P. 2010, MNRAS, 404, 1464
 Okvirik, P., Pichon, C., & Teyssier, R. 2008, MNRAS, 390, 1326
 Oosterloo, T., Fraternali, F., & Sancisi, R. 2007, AJ, 134, 1019
 Panter, B., Jimenez, R., Heavens, A. F., & Charlot, S. 2007, MNRAS, 378, 1550
 Patton, D. R., Carlberg, R. G., Marzke, R. O., et al. 2000, ApJ, 536, 153
 Pisano, D. J., Barnes, D. G., Gibson, B. K., Staveley-Smith, L., Freeman, K. C., & Kilborn, V. A. 2007, ApJ, 662, 959
 Pisano, D. J., Barnes, D. G., Staveley-Smith, L., et al. 2011, ApJS, 197, 28
 Portinari, L., Sommer-Larsen, J., & Tantalo, R. 2004, MNRAS, 347, 691
 Prochaska, J. X., & Wolfe, A. M. 2009, ApJ, 696, 1543
 Putman, M. E., Peek, J. E. G., & Jong, M. R. 2012, ApJ, 749, 181
 Rand, R. J., & Benjamin, R. A. 2008, ApJ, 676, 991
 Roberts, M. S. 1975, in Sandage, A., ed, Galaxies and the Universe, University of Chicago Press, p. 309
 Robotham, A. S. G., Baldry, I. K., Bland-Hawthorn, J., et al. 2012, MNRAS, 424, 1448
 Sakai, S., Mould, J. R., Hughe, S. M. G., et al. 2000, ApJ, 529, 2, 698
 Sancisi, R., Fraternali, F., Oosterloo, T., & van der Hulst, T. 2008, A&ARv, 15, 189
 Shull, J. M., Jones, J. R., Danforth, C. W., & Collins, J. A. 2009, ApJ, 699, 754
 Shull, J. M., Smith, B. D., & Danforth, C. W. 2012, ApJ, 759, 15
 Stewart, K. R., Bullock, J. S., Wechsler, R. H., & Maller, A. H. 2009, ApJ, 702, 307
 Taylor, C. L., Koblunick, H. A., & Skillman, E. D. 1998, AJ, 116, 2746
 Tully, R. B., Rizzi, L., Shaya, E. J., et al., 2009, AJ, 138, 323
 Tully, R. B., Courtois, H. M., Dolphin, A. E., et al. 2013, AJ, 146, 86
 Tumlinson, J., Thom, C., Werk, J. K., et al. 2013, ApJ, 777, 59
 van der Hulst, J. M., van Albada, T. S., & Sancisi, R. 2001, in Hibbard, J. E., Rupen, M., van Gorkom J. H., eds, ASP Conf. Ser. Vol. 240, Gas and Galaxy Evolution, Astron. Soc. Pac. San Francisco, p. 451
 Verheijen M. A. W., Oosterloo T. A., van Cappellen W. A., et al. 2008, in Minchin R., Monjjan E., eds, AIP Conf. Ser. Vol. 1035, The Evolution of Galaxies Through the Neutral Hydrogen Window, Am. Inst. Phys., New York, p. 265
 Wakker, B. P., York, D. G., Howk, J. C., et al. 2007, ApJL, 670, L113
 Whiting, M. T. 2012, MNRAS, 421, 3242
 Zwaan, M. A., Meyer, M. J., Staveley-Smith, L., & Webster, R. L. 2005, MNRAS, 359, L30

Appendix A: Global properties of the main galaxies

In this Appendix, we list the main properties of the spiral galaxies selected from the WHISP sample for this work. Columns as follows.

Column (1) gives the UGC name.

Column (2) provides an alternative common name, like NGC, DDO or IC classifications.

Column (3) provides the adopted distance in Mpc. We preferably used the EDD catalogue (Tully et al. 2009), otherwise, we used the following distance sources, in the given order: Cosmicflows-2 (Tully et al. 2013), NED archive, Hubble flow with $H_0 = 70 \text{ km s}^{-1} \text{ Mpc}^{-1}$ and systemic velocities corrected for Virgo-infall taken from the HyperLEDA catalogue.

Columns (4) and (5) give the radius R_{25} , namely the length of the projected semi-major axis of a galaxy at the isophotal level 25 mag arcsec⁻² in the B-band. R_{25} is taken from the HyperLEDA catalogue. In Col. (4) the radius is in arcminutes, in Col. (5) is converted in kiloparsecs using the distances in Col. (3).

Column (6) provides the inclination angle derived from the axis ratio in B-band as listed in the HyperLEDA catalogue.

Column (7) gives the systemic velocity measured in this work as the average midpoint between the velocities at the 20% and 50% of the peak flux of the global HI-line profile.

Column (8) gives the H α -line width at the 20% of the peak flux of the global H α -line profile, as calculated in this work.

Column (9) provides the total H α mass estimated in this work.

Column (10) gives the adopted total baryonic mass M_{bar} , calculated as described in section 2.3.

Column (11) provides the star formation rate calculated from the 60 μm and 100 μm IRAS fluxes.

Column (12) gives the total gas accretion rate from minor mergers estimated in this work, including detectable and “hidden” accretion.

Table A.1. Global properties of the main galaxies selected from the WHISP sample.

UGC name	Other name	D Mpc	R_{25} '	R_{25} kpc	i °	v_{sys} km/s	w_{20} km/s	M_{HI} $10^9 M_{\odot}$	M_{bar} $10^9 M_{\odot}$	SFR M_{\odot}/yr	\dot{M}_{HI} M_{\odot}/yr
(1)	(2)	(3)	(4)	(5)	(6)	(7)	(8)	(9)	(10)	(11)	(12)
UGC 00094	NGC 0026	68.6 ¹	0.56	11	47	4587	320	9.63	53.34	1.17	0.04
UGC 00232	-	65.3 ²	0.52	10	51	4837	275	7.61	38.40	1.95	0.10
UGC 00485	-	58.9 ¹	1.15	20	83	5246	357	21.63	45.84	1.27	0.90
UGC 00528	NGC 0278	12.0	1.17	4	20	640	138	1.32	15.68	1.02	0.01
UGC 00624	NGC 0338	78.3 ¹	0.87	20	68	4770	560	15.61	173.95	5.14	1.09
UGC 00625	IC 0065	28.3	1.29	11	73	2628	360	7.68	27.05	1.12	0.74
UGC 00690	-	74.5 ¹	0.85	18	46	5872	325	9.61	56.80	0.54	0.64
UGC 00731	-	12.0	0.93	3	24	639	143	0.88	38.54 ⁴	0.21	0.01
UGC 00798	IC 1654	69.4 ²	0.50	10	40	4898	222	3.96	43.96	0.60	0.11
UGC 01013	NGC 0536	62.5 ¹	1.48	27	69	5187	525	8.26	109.87	1.25	0.28
UGC 01256	NGC 0672	8.3	3.54	9	67	431	240	7.56	13.99	0.18	0.01
UGC 01437	NGC 0753	54.5 ²	0.69	11	51	4905	339	11.58	83.23	4.09	1.74
UGC 01550	NGC 0801	52.2 ¹	1.38	21	78	5764	470	15.86	75.68	2.33	0.17
UGC 01633	NGC 0818	58.1 ¹	1.09	18	70	4258	501	11.35	88.10	2.57	0.21
UGC 01810	-	109.8 ³	0.87	28	69	7578	602	31.64	210.16	2.37	0.88
UGC 01856	-	41.3 ²	1.07	13	81	4804	270	11.37	21.89	0.23	0.07
UGC 01886	-	67.4 ²	0.26	5	57	4854	502	25.67	121.29	0.85	0.33
UGC 01913	NGC 0925	9.2	5.36	14	58	552	222	3.85	12.90	0.64	<0.01
UGC 01993	-	107.7 ¹	0.89	28	75	8018	526	13.70	95.49	1.24	1.03
UGC 02045	NGC 0972	21.7	1.66	10	61	1525	332	2.12	45.93	4.42	<0.01
UGC 02069	-	36.6 ¹	0.62	7	55	3780	255	4.15	17.71	1.10	0.07
UGC 02080	IC 0239	10.0	2.13	6	24	902	135	5.46	11.52	0.16	0.01
UGC 02082	-	14.7	2.56	11	79	702	215	1.36	4.64	0.04	0.01
UGC 02141	NGC 1012	24.7	1.04	8	60	987	233	2.20	17.53	1.36	1.33
UGC 02154	NGC 1023	10.2	3.71	11	70	695	482	2.21	44.83	0.78	0.01
UGC 02183	NGC 1056	21.7	0.93	6	61	1540	290	3.65	18.80	0.98	0.01
UGC 02459	-	32.4	1.17	11	83	2467	337	12.30	31.48	0.59	1.28
UGC 02487	NGC 1167	72.2 ³	0.91	19	41	4953	468	16.65	261.23	3.21	1.36
UGC 02503	NGC 1169	32.4	1.66	16	54	2391	461	9.69	95.99	1.12	0.12
UGC 02800	-	18.9 ¹	1.17	6	60	1187	217	2.01	5.05	1.52	0.25
UGC 02855	-	14.4 ¹	1.77	7	65	1196	453	6.35	49.22	2.22	0.02
UGC 02916	-	68.0 ²	0.66	13	24	4517	336	23.12	94.12	2.45	1.40
UGC 03013	NGC 1530	25.4	0.91	7	55	2459	341	8.98	53.03	2.07	0.03
UGC 03137	-	22.1	1.90	12	78	993	216	4.41	9.32	0.15	0.02
UGC 03205	-	47.6 ²	0.66	9	66	3588	436	9.21	65.30	0.95	2.18
UGC 03326	-	77.6 ¹	1.66	37	84	4060	532	19.48	135.84	2.38	0.05
UGC 03334	NGC1961	59.5 ³	2.23	39	50	3935	660	39.72	422.71	9.24	0.26
UGC 03354	-	52.5 ¹	0.83	13	70	3085	441	8.89	68.85	3.22	0.02
UGC 03382	-	67.2 ³	0.63	12	21	4501	205	5.74	73.75	0.76	0.34
UGC 03407	-	39.3 ²	0.56	6	45	3602	312	1.75	22.06	0.70	1.17
UGC 03422	-	77.2 ²	0.91	20	62	4065	416	11.05	73.40	1.08	1.00
UGC 03546	NGC 2273	17.9	1.15	6	53	1836	339	1.95	19.09	0.56	0.21
UGC 03574	-	17.1	0.74	4	30	1441	150	3.21	6.70	0.35	0.02
UGC 03580	-	25.9	1.07	8	57	1198	236	3.81	12.87	0.48	0.02
UGC 03642	-	67.4 ²	0.76	15	41	4498	410	37.21	146.52	1.99	0.89
UGC 03734	NGC 2344	23.0	1.02	7	24	972	150	1.12	14.80	0.11	0.01
UGC 03759	NGC 2347	88.3 ¹	0.83	21	44	4416	468	22.39	200.89	5.72	0.40
UGC 03993	-	66.3 ³	0.42	8	24	4365	175	7.13	50.87	0.91	0.04
UGC 04036	NGC 2441	44.7 ¹	1.00	13	24	3469	141	4.07	31.61	0.89	0.11
UGC 04165	NGC 2500	15.0	1.23	5	25	515	113	0.97	6.82	0.35	<0.01
UGC 04256	NGC 2532	51.6 ²	0.83	12	34	5256	175	6.73	56.96	3.70	0.10
UGC 04273	NGC 2543	26.3	1.23	9	62	2473	317	4.32	20.75	1.23	0.11
UGC 04284	NGC 2541	11.2	1.51	5	59	559	210	4.91	8.32	0.08	<0.01
UGC 04458	NGC 2599	68.6 ³	0.77	15	32	4757	285	12.52	128.09	1.39	1.09
UGC 04605	NGC 2654	22.7	2.23	15	78	1354	430	6.32	35.50	0.82	0.01

UGC 04666	NGC 2685	16.0	2.18	10	58	876	303	1.96	17.39	0.14	0.22
UGC 04806	NGC 2770	25.5	1.73	13	76	1945	353	5.42	19.53	0.64	0.85
UGC 04838	NGC 2776	36.0	1.07	11	65	2626	202	6.24	44.41	1.53	0.03
UGC 04862	NGC 2782	42.1	1.62	20	42	2540	196	4.12	67.81	4.49	0.01
UGC 05060	NGC 2893	24.0	0.51	4	36	1700	187	0.92	6.66	0.42	0.05
UGC 05079	NGC 2903	8.5	6.01	15	63	555	390	3.95	39.88	0.95	<0.01
UGC 05251	NGC 3003	19.6 ¹	2.39	14	77	1481	294	8.89	20.10	0.40	0.02
UGC 05253	NGC 2985	16.6	1.82	9	36	1324	316	11.62	55.21	0.82	0.37
UGC 05351	NGC 3067	20.6	1.02	6	71	1487	281	0.91	15.67	1.17	0.01
UGC 05452	NGC 3118	20.6	1.04	6	78	1348	216	3.41	5.91	0.07	0.02
UGC 05459	-	25.8	1.90	14	79	1108	282	4.82	18.06	0.48	0.02
UGC 05532	NGC 3147	39.8	2.04	24	29	2812	390	9.50	227.06	4.95	0.13
UGC 05556	NGC 3187	26.4	1.12	9	71	1582	276	1.09	5.48	0.48	0.06
UGC 05557	NGC 3184	13.0	3.71	14	21	593	146	3.95	32.47	0.20	0.01
UGC 05589	NGC 3206	25.8	1.15	9	59	1162	182	2.61	6.50	0.03	0.06
UGC 05685	NGC 3254	21.8	1.17	7	72	1359	378	4.71	24.34	0.22	0.10
UGC 05717	NGC 3259	24.0	0.85	6	58	1675	242	6.34	14.71	0.43	0.05
UGC 05786	NGC 3310	20.0	0.95	6	40	989	221	3.36	17.42	3.23	0.02
UGC 05789	NGC 3319	13.3	1.82	7	61	739	215	3.36	6.76	0.06	0.01
UGC 05840	NGC 3344	10.0	3.38	10	25	589	175	3.01	17.40	0.25	<0.01
UGC 05906	NGC 3380	26.1	0.77	6	27	1600	130	0.42	9.70	0.15	0.01
UGC 05909	NGC 3381	25.7	1.00	7	26	1633	146	2.12	9.07	0.34	0.02
UGC 05918	-	10.0	1.23	4	12	338	78	0.25	0.57	0.09	<0.01
UGC 05997	NGC 3403	20.2	1.38	8	68	1261	303	4.09	12.89	0.46	0.03
UGC 06024	NGC 3448	24.0	1.48	10	73	1369	299	6.76	21.06	1.12	0.05
UGC 06128	NGC 3512	26.1	0.79	6	29	1388	187	0.98	13.03	0.35	0.01
UGC 06225	NGC 3556	9.6	1.99	6	65	698	341	3.48	22.10	0.81	0.02
UGC 06263	NGC 3583	33.0	1.12	11	56	2134	346	6.65	69.34	2.59	0.07
UGC 06283	NGC 3600	14.4	0.93	4	72	713	218	2.86	6.14	0.26	0.01
UGC 06537	NGC 3726	17.1	2.62	13	47	864	284	5.05	35.11	0.46	0.01
UGC 06621	NGC 3786	40.0	0.97	11	59	2745	418	4.56	42.88	1.27	0.02
UGC 06778	NGC 3893	17.1	1.35	7	58	968	311	4.76	31.95	1.59	0.99
UGC 06786	NGC 3900	22.5	1.29	8	61	1801	426	3.33	25.43	0.24	0.56
UGC 06787	NGC 3898	22.1	1.73	11	54	1170	446	3.96	57.99	0.96	1.12
UGC 06833	NGC 3930	12.6	1.35	5	42	918	161	0.99	7.00	0.36	0.01
UGC 06870	NGC 3953	19.2 ¹	3.09	17	62	1051	403	2.35	72.36	0.30	0.09
UGC 06884	NGC 3963	49.1 ²	1.26	18	27	3189	131	8.21	68.56	1.76	0.09
UGC 06930	-	17.1	0.71	4	42	778	141	2.52	4.77	0.19	0.01
UGC 06964	NGC 4010	19.1 ¹	1.55	9	78	905	278	1.40	8.52	0.28	0.01
UGC 07030	NGC 4051	17.2	2.45	12	40	704	241	1.43	33.28	0.86	0.01
UGC 07081	NGC 4088	14.5 ¹	3.54	15	68	756	381	4.15	32.18	1.51	0.01
UGC 07095	NGC 4100	20.3 ¹	2.29	14	74	1075	402	3.02	35.53	1.21	0.03
UGC 07183	NGC 4157	18.0	3.08	16	80	771	422	6.29	54.12	1.69	0.03
UGC 07222	NGC 4183	16.4 ¹	2.13	10	81	931	247	2.95	7.98	0.20	0.01
UGC 07256	NGC 4203	15.1	1.69	7	65	1088	270	2.34	33.99	0.10	<0.01
UGC 07321	-	6.0	2.39	4	86	407	210	0.34	0.72	0.08	0.01
UGC 07399	NGC 4288	9.2	0.85	2	41	535	165	0.74	1.35	0.35	0.01
UGC 07483	NGC 4359	16.3	0.69	3	53	1271	199	1.13	3.14	0.21	0.01
UGC 07489	NGC 4369	11.2	1.00	3	17	1029	88	0.43	4.83	0.33	0.02
UGC 07506	NGC 4384	36.0	0.63	7	39	2532	176	1.13	12.87	0.84	0.20
UGC 07766	NGC 4559	8.7	5.24	13	63	814	256	5.43	16.21	0.22	<0.01
UGC 07989	NGC 4725	12.4	4.89	18	45	1210	398	5.02	71.56	1.06	1.03
UGC 08307	NGC5033	19.1 ¹	9.77	54	65	875	425	10.43	88.98	1.76	1.27
UGC 08403	NGC 5112	18.5	1.51	8	52	969	215	3.12	8.53	0.35	0.01
UGC 08699	NGC 5289	30.9	1.17	11	72	2518	352	2.76	18.81	0.23	0.02
UGC 08709	NGC 5297	30.9	1.86	17	76	2405	414	12.73	50.61	1.05	0.09
UGC 08711	NGC 5301	20.2	1.99	12	78	1508	336	3.56	18.33	0.81	0.04
UGC 08863	NGC 5377	28.0	1.82	15	67	1791	382	2.24	47.16	0.42	0.01
UGC 08900	NGC 5395	52.7 ²	1.26	19	62	3458	565	11.21	143.67	3.53	0.25
UGC 09242	-	27.9	2.08	17	86	1438	215	3.20	6.43	0.21	0.01
UGC 09366	NGC 5676	38.9	1.82	21	63	2121	462	6.41	137.46	5.76	1.09
UGC 09431	NGC 5714	38.7 ¹	1.41	16	80	2242	356	7.51	29.58	0.66	0.14
UGC 09644	-	97.9 ³	0.57	16	20	6664	136	7.12	42.84	1.28	0.11

UGC 09753	NGC 5879	15.5	1.90	9	68	771	287	1.32	10.88	0.28	0.01
UGC 09797	NGC 5905	46.6 ¹	1.62	22	50	3393	374	22.70	73.72	2.56	1.25
UGC 09858	-	32.2	1.95	18	78	2615	386	10.67	28.75	0.41	1.66
UGC 09969	NGC 5985	43.7	1.99	25	60	2515	542	10.76	144.58	1.19	0.14
UGC 10359	NGC 6140	16.0	1.04	5	44	908	221	5.41	11.61	0.14	0.01
UGC 10445	-	18.1	0.95	5	45	962	159	2.23	6.94	0.16	0.05
UGC 10448	NGC 6186	154.0 ²	0.79	35	41	11352	118	9.56	439.96	8.82	0.02
UGC 10470	NGC 6217	23.0	1.12	7	34	1355	192	5.94	30.66	1.86	0.02
UGC 10497	-	65.6 ²	0.59	11	65	4296	267	8.93	21.34	0.36	0.17
UGC 10564	NGC 6237	21.0	0.62	4	52	1129	175	5.64	11.08	0.27	0.03
UGC 11124	-	25.0	1.12	8	26	1599	153	2.23	11.71	0.16	0.03
UGC 11218	NGC 6643	20.6	1.66	10	61	1484	350	3.20	30.27	1.78	0.04
UGC 11269	NGC 6667	44.9	0.93	12	56	2581	412	13.36	66.90	1.73	0.02
UGC 11283	IC 1291	30.0	0.66	6	35	1946	198	2.55	9.44	0.38	0.55
UGC 11429	NGC 6792	62.2 ¹	1.04	19	58	4637	510	12.26	129.81	1.60	0.31
UGC 11466	-	18.1	0.74	4	53	821	237	2.79	10.96	0.84	0.01
UGC 11670	NGC 7013	15.0	2.08	9	71	775	340	1.35	26.16	0.28	<0.01
UGC 11852	-	82.4 ²	0.46	11	44	5845	328	26.73	82.67	0.96	0.45
UGC 11861	-	14.4	0.89	4	61	1482	259	2.10	10.25	0.47	0.02
UGC 11909	-	14.1	1.00	4	78	1105	242	2.87	7.78	0.39	0.01
UGC 11914	NGC 7217	15.0	2.29	10	35	950	301	0.70	52.88	0.68	<0.01
UGC 11951	NGC 7231	14.2	0.85	4	69	1086	223	1.56	4.97	0.35	0.92
UGC 11994	-	65.8 ¹	1.04	20	82	4882	436	6.95	57.44	1.69	0.29
UGC 12554	NGC 7640	9.9	4.06	12	78	363	238	3.05	8.78	0.24	<0.01
UGC 12693	-	60.5 ¹	0.55	10	78	4958	236	9.67	15.50	0.69	0.12
UGC 12732	-	15.1	1.38	6	28	728	131	1.96	4.06	0.59	0.01
UGC 12754	NGC 7741	13.6 ¹	1.82	7	49	749	202	1.78	5.76	0.36	0.01
UGC 12808	NGC 7769	61.5 ³	0.87	16	68	4225	326	4.79	134.32	6.21	0.05

¹ Distance from Cosmicflows-2 catalogue.² Distance from NED catalogue.³ Distance from Hubble flow with Virgo infall corrected systemic velocity.⁴ Baryonic mass from baryonic Tully-Fisher relation.